Journal of Molecular Spectroscopy **214,** 80–86 (2002)
doi:10.1006/jmsp.2002.8578

The $T_1 \leftarrow S_0$ Absorption Spectrum of Gaseous 4H-Pyran-4-thione

A. A. Ruth,*,[1] T. Fernholz,† R. P. Brint,* and M. W. D. Mansfield‡

*Department of Chemistry, National University of Ireland, University College Cork, Cork, Ireland; †Institut für Physikalische Chemie, Universität Heidelberg, Im Neuenheimer Feld 234, 69120 Heidelberg, Germany; and ‡Department of Physics, National University of Ireland, University College Cork, Cork, Ireland

Received February 19, 2002; in revised form April 4, 2002

IN MEMORY OF DR. BERNHARD NICKEL

The $T_1 \leftarrow S_0$ absorption spectrum of 4H-pyran-4-thione (PT) was measured in a static cell at room temperature (550–620 nm) and in a seeded cold supersonic jet (580–600 nm) using the cavity ring-down (CRD) method. In the static cell absolute extinction coefficients were determined between 573 and 610 nm with an accuracy of $\sim\pm5\%$. In this region 22 harmonic sequences and 18 hot bands were observed. The energetically lowest ground state vibration at 167.5 cm^{-1} was identified as the promoting mode in the static PT gas. The mode in the triplet state was found at 152.3 cm^{-1}. The CRD absorption spectra of static PT gas and jet-cooled PT are compared with the phosphorescence excitation spectrum of isolated PT. The weak $S_{1,0} \leftarrow S_{0,0}$ absorption was tentatively assigned to a transition at $\sim$17433 cm^{-1}.

Key Words: aromatic thiocarbonyls; 4H-pyrane-4-thione; PT; triplet state; cavity ring-down spectroscopy; absorption.

INTRODUCTION

The metastable first excited triplet state T_1 of aromatic thiocarbonyl compounds has been widely studied over the last few decades (*1*). The majority of photophysical and photochemical investigations on T_1 of thioketones consider molecules in solution at room temperature and in rigid matrices at low temperatures. In order to obtain information on triplet manifolds in large *gaseous* thioketones we recently discussed various aspects of the $T_1 \leftarrow S_0$ transition in *jet-cooled* 4H-1-benzopyran-4-thione (BPT) in several publications (*2–4*). In Ref. (*4*) we demonstrated that, using conventional pulsed cavity ring-down (CRD) spectroscopy (*5*) it is possible to investigate spin-forbidden singlet–triplet absorptions with an oscillator strength $\lesssim 10^{-4}$ in a supersonic jet. Encouraged by the successful measurements on BPT, the present investigation focusses on the $T_1 \leftarrow S_0$ transition in gaseous 4H-pyran-4-thione (PT, shown in Fig. 1), which possesses a higher vapor pressure than BPT. Thus, CRD absorption spectra were recorded for static gaseous PT at room temperature in particular, apart from measurements of PT in a cold supersonic jet. The motivation for this investigation is twofold:

(i) Apart from the phosphorescence excitation spectrum of jet-cooled PT (*6*), the triplet manifold of PT has so far only been studied in the condensed phase (*7–11*) and recently in a novel theoretical approach concerning spin-forbidden transitions (*12*). None of the $T_1 \leftarrow S_0$ absorption spectra presented here has been recorded before. In particular no information on static gaseous PT exists. The expected complex structure in the highly congested absorption spectrum of "warm" static PT gas is of interest since it contains information on the low energy fundamental modes in the PT ground state S_0, which were only calculated so far, but could not be observed experimentally in IR and Raman spectra (*13*). The comparison of the absorption spectra of PT in a static cell and jet-cooled PT in conjunction with the phosphorescence excitation spectrum in Ref. (*6*) facilitates the analysis of hot bands, from which information on the S_0 vibrational structure and assignments in the T_1 vibronic manifold can be extracted.

(ii) The number of new systems studied using cavity enhanced absorption methods has greatly increased over the last few years; several reviews have been published (*14–17*). In this application of pulsed CRD spectroscopy the difficulties involved in monitoring the outgasing of volatile solid materials *quantitatively* will be outlined. A method to evaluate absolute concentrations, despite the resublimation and heterogeneous elimination of gaseous PT, will be discussed in the experimental section.

EXPERIMENT

The Cavity Ring-Down Apparatus

The experimental setup is shown schematically in a previous publication (Fig. 1a in Ref. (*4*)), thus only a short description of the apparatus is given here. The ring-down cavity consisted of two highly reflecting plano-concave mirrors with a specified reflectivity of $R \gtrsim 99.99\%$ between 580 and 640 nm (diameter 25.4 mm, radius of curvature 2 m). The mirrors were mounted on adjustable bellows at the end of a vacuum chamber with a length of $l \approx 770.5$ mm. For an evacuated cavity the longest ring-down time of $\tau_{crd} = 68\ \mu s$ was found at $\sim$610 nm, which corresponds to $R = 0.99996$. The excitation light source was an excimer-pumped pulsed dye laser (Lumonics EX-700, XeCl;

[1] To whom correspondence should be addressed. E-mail: a.ruth@ucc.ie.

0022-2852/02 $35.00

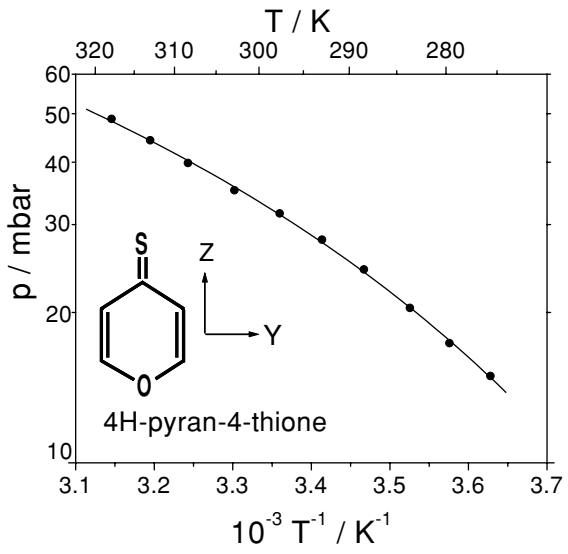

FIG. 1. Temperature dependence of the vapor pressure of 4H-pyran-4-thione. The solid line was calculated with the Antoine Eq. [1] using the parameters A = 2.529, B = 94.609 K, and C = −205.977 K, which were calculated in a nonlinear least-squares fit.

Lumonics HD-300; rhodamine B) with a spectral resolution of $\lesssim 0.3$ cm^{-1}. The ratio of the pulse duration to the round trip time was approximately 3. The decay of the light intensity in the cavity was monitored with a red-sensitive photomultiplier (Philips XP2254/B), whose output signal at a medium photocathode voltage was measured directly with a digital oscilloscope (LeCroy 9410), which was interfaced to a computer. A linear regression of the central part of the logarithm of the low-pass filtered decay data yielded the ring-down time in a reliable and quick way (the treatment of the offset is discussed in Ref. (*4*)). Decay curves were typically sampled over 100 laser shots.

The Vapor Pressure and Molecular Concentration of PT Vapor

For the synthesis of PT the procedure in (*18*) was followed; it was further purified by several recrystallizations. The vapor pressure of PT was measured using the following procedure: PT was filled into a small glass flask which was connected to a capacitive membrane gauge head (Leybold CM 100) on one side and to a vacuum line on the other side. After several freeze–pump–thaw cycles the flask was melted off the vacuum line together with the gauge head. This closed system was then put into a brass container, which was subsequently densely packed with small brass chippings in order to guarantee good heat contact. The entire brass container was put into a thermostatic water bath (Haake Q/F3). The temperature was varied between 5° and 50°C; at each temperature more than 6 h were allowed for thermal equilibrium to be reached. The temperature dependence of the vapor pressure $p(T)$ of PT is shown in Fig. 1. The values for p are accurate within ±2 mbar and can be described by the Antoine equation (*19*)

$$\log(p/\text{mbar}) = \text{A} - \frac{\text{B}}{T + \text{C}}. \qquad [1]$$

Fitting Eq. [1] to the measured vapor pressures yielded the following parameters: A = 2.529 ± 0.083, B = 94.615 ± 14.575 K, and C = −205.974 ± 6.635 K. The solid line in Fig. 1 was calculated using these parameters.

The Jet Apparatus

For the supersonic jet experiment PT was seeded into ≈950 mbar helium at a temperature of ≈48°C and expanded into vacuum through a circular pulsed nozzle with a diameter of $D = 1.2$ mm (Iota One nozzle driver, General Valve). The position of the nozzle in the ring-down cavity was adjusted perpendicular to the optical axis of the resonator so that the signal of the $T_1 \leftarrow S_0$ absorption of PT was maximal. The supersonic jet was intercepted ∼4.8 mm downstream from the nozzle, where the translational temperature was estimated to be ≈14.8 K. A jet-pulse repetition rate of 6 Hz and a jet-pulse duration of 800 μs were used.

Evaluation of Absolute Extinction Coefficients in a Static Cell

One obvious difficulty in measuring absolute extinction coefficients of solid compounds in the gas phase at a particular temperature is the determination of the time-dependent concentration $c(t)$ of the substance in the gas phase. The following procedure describes the determination of absolute absorption coefficients of gaseous PT in a static cell: (i) τ_{crd}^{-1} was repetitively measured in the origin of the $T_1 \leftarrow S_0$ transition for approximately 160 minutes after filling PT into the vacuum chamber. The decay of the concentration of PT in the gas phase $c(t) = n(t)/V$ was monitored after a fast initial build up. A simple exponential $\sim\exp(-t/\tau_c)$ was fitted to the concentration decay, yielding a lifetime of $\tau_c \sim 21.63$ minutes. (ii) An accurate amount of 2.8 mg PT (corresponding to $n(0) = 2.5 \times 10^{-5}$ mol) was filled into the chamber. This amount represents less than 1% of the maximum that could be sublimed into the chamber, according to the PT vapor pressure (Fig. 1), the measured volume of the chamber $V = 5.055$ dm^3, and the ambient temperature. Therefore we are confident that initially the *full* amount of PT was present in the gas phase in step (ii). Under these conditions a measurement was performed at 16 different relevant wavelengths between 574 and 609 nm, where reasonably strong transitions are located. This experiment lasted ≈50 min. (iii) The absorbances $A(t)$ of this measurement were corrected according to the exponential time dependence of the precipitation of PT. The *absolute* extinction coefficients were then calculated using $\epsilon = (AV)/(n(t)l)$. (iv) The resulting 16 extinction values were used to scale a full spectrum through linear interpolation. The spectrum derived from this procedure is shown in the low energy part of Fig. 2 up to 17 450 cm^{-1}. The error of ϵ is estimated to be ±5%.

3. RESULTS AND DATA ANALYSIS

3.1. The Cavity Ring-Down Spectrum of the $T_1 \leftarrow S_0$ Transition of PT in a Static Cell

The $T_1 \leftarrow S_0$ cavity ring-down absorption spectrum of static PT gas at room temperature, shown in Fig. 2, was measured between 16 400 and 18 150 cm^{-1}. Over the entire spectral range the reciprocal ring-down times of the *empty* cavity were interpolated by a 4th-order polynomial (=mirror reflectivity curve). This curve was subtracted from the CRD absorption spectrum in Fig. 2. In the low energy part covering the region $\leq$17 450 cm^{-1} the spectrum was additionally corrected according to the procedure described in Section 2. The reciprocal ring-down times in the high energy part of the figure (>17 450 cm^{-1}) were not corrected and are distorted since the mirror reflectivities decrease very rapidly in this wavelength region. Subtraction of the mirror reflectivity curve, therefore, does not entirely compensate for the wavelength dependence of the mirror reflectivity and consequently the relative absorbances in this range have only qualitative character.

All assigned absorption features of the spectrum are due to transitions to the triplet substate $T_{1z}(A_1)$. Owing to symmetry restrictions the absorption transition moment of $T_{1x}(B_1)$ and $T_{1y}(B_2)$ is $\approx$140 times smaller than that of T_{1z} (*7*). Absorption lines were identified through comparison with the $T_1 \leftarrow S_0$ phosphorescence excitation (PE) spectrum of jet-cooled PT (*6*); those marked with an arrow in Fig. 2 are listed in Tables 1 and 2. In the previous publication (*6*) there is a confusion of the molecular axes used to determine the symmetry representations; i.e., the molecular plane was referred to as being the yz-plane in the text, and the xz-plane in Tables 1 and 2 in (*6*). This resulted in mislabelling the b_1 and b_2 symmetry vibrations and a few misassignments through comparison with (*13*). The axis convention used in this paper has the $z(a_1)$ axis along the C=S bond, $y(b_2)$ as the second in-plane coordinate, and $x(b_1)$ perpendicular to the molecular plane as shown in Fig. 1. All assignments presented here supercede those in Ref. (*6*).[2]

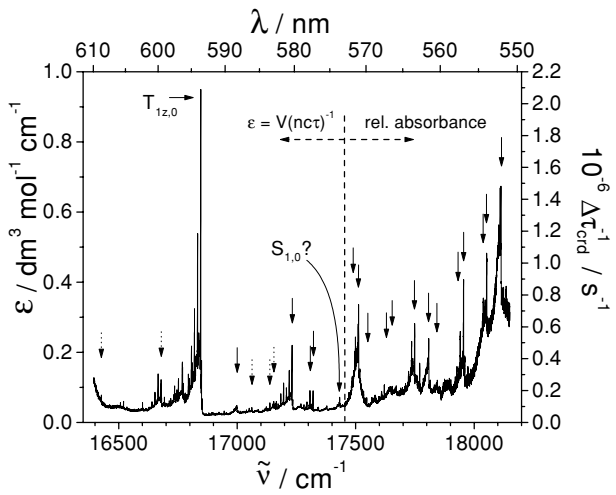

FIG. 2. Cavity ring-down absorption spectrum of PT at room temperature. The absolute extinction scale (ϵ, left axis) refers to the low energy part of the spectrum ($\leq$17 450); the relative absorbance scale ($\Delta\tau_{crd}^{-1}$, right axis) refers to the high energy part of the spectrum (>17 450). The solid arrows indicate positions of all fundamental vibrations which are listed in Tables 1 and 2 (assignments in comparison with Ref. (*6*)). The $T_{1z,0}$ origin and the alleged position of $S_{1,0}$ are shown explicitly. The dashed arrows indicate hot bands which are identified in Table 1. Excitation wavenumbers are vacuum corrected.

All but one of the T_{1z} fundamental and combination lines from the PE spectrum were reproduced (the one exception being at 815 cm^{-1} above $T_{1z,0}$). Shifts of the line maxima $|\Delta\tilde{\nu}|$ between 1 and 5 cm^{-1} were observed and are due to the large difference in the rotational temperature between the jet and the static cell experiment. This aspect is further discussed in Section 3.3 (see Fig. 5 in Section 3.3).

In the low energy part of the spectrum a total of 118 lines were observed. Most of them are either members of 22 harmonic sequences or hot bands; some are single lines. Assignments are listed in Table 1, where sequence origins are marked with an "o.". Almost all absorption lines in the table are either stronger than 5% of the $T_{1z,0} \leftarrow S_{0,0}$ transition at 16 846 cm^{-1}, and/or they are the member of a progression. In principle also the absorption of the substates T_{1x} and T_{1y}, whose absorption transition moment is $\approx$140 times smaller than that of T_{1z} (*7*), contributes to the static cell spectrum. Although the signal-to-noise ratio is large enough to detect the weak absorption of T_{1x} and T_{1y} in the static cell experiment, the spectrum obtained at room temperature is too congested at excitation energies $|D^*| \approx$ 24–28 cm^{-1} below $T_{1z,0}$, where the $T_{1(xy),0} \leftarrow S_0$ transitions are located according to matrix ODMR measurements (*7*). This region is indicated by a double arrow ($\leftrightarrow$) in Fig. 5.

Since the vast majority of lines in Fig. 2 are due to hot bands at room temperature (T $\approx$ 298 K) and their associated progressions, it is important to unambiguously assign the energetically lowest fundamental modes in the ground and the excited state in order to characterize the spectrum. Data on ground state vibrations are published in Ref. (*13*); however, the lowest energy modes were either only determined from spectra in a melt or calculated. In the following we will justify our assignment of the lowest energy out-of-plane ring mode $\nu_{18}(b_1) \sim 167$ cm^{-1} (S_0) in the ground state and $\nu_{18}(b_1) \sim 152$ cm^{-1} (T_{1z}) in the first excited triplet state.

The Lowest Ground State Mode $S_{0,\nu_{18}}$ (b_1)

The strongest observed hot band below the 0,0 transition (12.8% of the intensity of the 0,0 transition), located at -167.5 cm^{-1}, is due to the lowest energy mode ν_{18} in the ground state. It is the origin of a long harmonic sequence. Under ideal conditions this vibration can be populated up to 44% at 298 K.

[2] Herzberg's numbering scheme is followed (*20*); i.e., within a given symmetry species vibrations are numbered starting with the highest frequency—for PT, $a_1 = \nu_1 \ldots \nu_9$, $a_2 = \nu_{11} \ldots \nu_{13}$, $b_1 = \nu_{14} \ldots \nu_{18}$, $b_2 = \nu_{19} \ldots \nu_{27}$.

TABLE 1
Spectroscopic Data on the Vibronic Transitions $T_{1z,\nu} \leftarrow S_{0,\nu}$ of PT in a Static Cell

T_1 Assignments						
			Sequence parameter			
$\tilde{\nu}$ (T_{1z,ν_i}) [cm^{-1}]	$T_{1z,\nu_i} - T_{1z,0}$ [cm^{-1}]	Rel. abs. %	Extr. orig. [cm^{-1}]	Spacing [cm^{-1}]	No. of lines	Assignment
16427.1	−419.3 o.	8.2	16427.1	−13.48	2	$T_{1z,0}(A_1) \leftarrow S_{0,\nu_{27}}(b_2)$
16462.0	−384.4	5.3				
16497.3	−349.1	5.1				
16520.5	−325.9 o.	6.3	16520.5	−13.08	3	
16600.5	−245.9 o.	5.9	16600.6	−16.50	3	
16641.7	−204.7 o.	5.4	16641.8	−12.19	4	
16671.7	−174.7	7.6				
16676.4	−170.0 o.	9.5	16676.4	−13.33	3	
16678.9	−167.5 o.	12.8	16679.1	−12.85	6	$T_{1z,0}(A_1) \leftarrow S_{0,\nu_{18}}(b_1)$
16681.1	−165.3 o.	7.5	16681.0	−12.02	4	
16693.1	−153.3	7.6				
16695.3	−151.1	5.9				
16737.8	−108.6 o.	7.8	16737.7	−11.05	3	
16745.7	−100.7 o.	9.8	16745.6	−11.95	4	
16768.7	−77.7 o.	18.2	16768.5	−16.16	5	
16810.7	−35.7*4 o.	18.0	16810.7	−12.54	5	
16846.4	0.0*1 o.	100.0	16846.3	−13.00	6	Origin $T_{1z,0}(A_1)$
16849.8	3.4*3 o.	18.6	16849.9	−11.89	5	
16852.6	6.2	6.9				
16995.2	148.8*6 o.	4.8	16995.5	−8.96	5	
16998.7	152.3 o. f.	5.1	16998.8	−12.28	4	$T_{1z,\nu_{18}}(b_1) \leftarrow S_{0,0}(A_1)$
17061.9	215.5 o.	4.4	17062.2	−11.53	5	$T_{1z,\nu_{27}}(b_2) \leftarrow S_{0,\nu_{18}}(b_1)$
17138.3	291.9 o.	5.9	17138.2	−15.03	4	$T_{1z,\nu_{17}}(b_1) \leftarrow S_{0,\nu_{18}}(b_1)$
17151.5	305.1	5.6				$T_{1z,\nu_{10}}(a_1) \leftarrow S_{0,\nu_{18}}(b_1)$
17153.5	307.1	5.8				
17154.4	308.0	6.3				
17157.1	310.7	5.3				
17165.0	318.6	6.3				
17180.7	334.3	5.1				
17215.6	369.2	7.7				
17216.4	370.0	7.6				
17221.2	374.8 o.	7.3	17221.1	−11.02	4	
17227.4	381.0	9.1				
17231.6	385.2*2 o. f.	23.2	17231.6	−11.82	7	$T_{1z,\nu_{27}}(b_2) \leftarrow S_{0,0}(A_1)$
17234.8	388.4 o.	6.9	17235.0	−10.62	6	
17307.3	460.9*5 o. f.	9.6	17307.4	−12.69	5	$T_{1z,\nu_{17}}(b_1) \leftarrow S_{0,0}(A_1)$
17311.8	465.4	5.3				
17316.6	470.2 o. f.	5.6	17316.7	−12.50	7	$T_{1z,\nu_{10}}(a_1) \leftarrow S_{0,0}(A_1)$
17320.2	473.8	9.5				
17432.5	586.1	7.6				Origin? $S_{1,0}(A_2)$

Note. $\tilde{\nu}$ (T_{1z,ν_i}), center wavenumbers; $T_{1z,\nu_i} - T_{1z,0}$, wavenumber difference to origin; Rel. abs., relative absorbance in % of the 0,0 transition; Extr. orig., extrapolated origin of sequence in [cm^{-1}]; Spacing, difference between lines in sequence in [cm^{-1}]; classification, o. = origin of sequence, f. = fundamental, *n = sequence n in Fig. 3. Symmetry assignments are taken from Ref. (*13*). All values of wavenumbers are vacuum corrected throughout the paper. The error limit of absolute wavenumbers is $\lesssim$4 cm^{-1}.

Since the next ground state fundamental mode ν_{27} at around 300 cm^{-1} (*13*) can at most be populated to $\approx$22%, the dominating mode in the static cell spectrum will be ν_{18}. In principle, however, vibrations up to 620 cm^{-1} can significantly contribute to features and progressions in the spectrum as they can be populated up to 5% of the ground state at room temperature. These states are likely to cause weak (not progression forming) hot bands, for instance between 300 and 370 cm^{-1} above the origin (cf. Table 1). Being the lowest energy mode, ν_{18} is expected to play an important role in the spectrum, since most sequences in Fig. 2 should be based on it. This is demonstrated in Fig. 3, where the relative absorbances of lines of 6 different sequences are plotted semilogarithmically versus their respective order in a sequence. In Fig. 3 the relative absorbances

TABLE 2
List of T_1 Vibronic States above 17 450 cm^{-1} in the Static Cell Spectrum

T_1 assignments			
$\tilde{\nu}$ ($T_{1z,\nu}$) [cm^{-1}]	$T_{1z,\nu_i} - T_{1z,0}$ [cm^{-1}]	Assignment T_1 manifold	Comparison $\Delta\tilde{\nu}$ [cm^{-1}]
17512.4	666.0	ν_{26} (b_2)	2.5
17517.6	671.2	ν_{16} (b_1)	−1.8
17547.1	700.9	ν_9 (a_1)	3.6
17621.5	775.1	$2\nu_{27}$	4.6
17638.9	792.5	ν_{12} (a_2)	−1.3
not obs.	(815)	ν_{15} (b_1)	
17689.6	843.2	$\nu_{27} + \nu_{17}$	−2.4
17706.8	860.4	$\nu_{27} + \nu_{10}$	4.7
17748.9	902.5	ν_8 (a_1)	3.5
17770.4	924.0	$2\nu_{17}$	4.5
17785.4	939.0	$\nu_{17} + \nu_{10}$	8.8
17808.3	961.9	ν_{11} (a_2)	3.5
17844.7	998.3	ν_{14} (b_1)	3.1
17885.7	1039.3	$\nu_{27} + \nu_{26}$	−7.0
17901.6	1055.2	$\nu_{27} + \nu_{16}$	−3.2
17927.4	1081.0	$\nu_{27} + \nu_9$	−3.1
17955.3	1108.9	ν_7 (a_1)	3.5

Note. Symmetry assignments in column 3 are based on results in Ref. (*13*). The last column shows $\Delta\tilde{\nu}$, which corresponds to the deviations of the center wavenumbers of lines found in the static cell CRD spectrum and in the $T_1 \leftarrow S_0$ phosphorescence excitation spectrum in Ref. (*6*).

represent the differences between the absorption maximum of a line in a sequence to the local rotational background, since strongly overlapping rotational branches from adjacent lines (particularly those outside a respective sequence) can significantly disturb the relative absorbances. The relative absorbances in all sequences decrease approximately exponentially, based on the energy of $\approx hc \times 156 \pm 29$ cm^{-1} at $T = 298$ K. This value was determined for the strongest sequence which is based on the origin $T_{1z,0} \leftarrow S_{0,0}$ transition, represented by the dotted line in Fig. 3 (the error is the standard deviation of the six sequences shown). A purely monoexponential behavior cannot be expected, because the Franck–Condon factors of transitions belonging to different orders are likely to be similar but not constant. Moreover, at higher order transitions of a sequence, the signal-to-noise ratio is much smaller (especially on top of a varying rotational background) and leads to apparent deviations from the monoexponential behavior. The value of ∼156 cm^{-1} is in acceptable agreement with the assignment of $\nu_{18} \sim 167.5$ cm^{-1} as the lowest energy mode in the ground state; it recurs in almost all sequences.

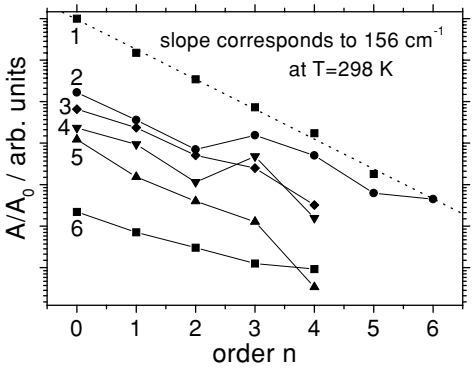

FIG. 3. Semilogarithmic plot of the relative absorbances of lines of 6 different harmonic sequences versus their order in the respective sequence. The dotted line represents a monoexponential function fitted to the datapoints. Origins of the sequences are 1: 16 846.4 cm^{-1}; 2: 17 231.6 cm^{-1}; 3: 16 849.8 cm^{-1}; 4: 16 810.7 cm^{-1}; 5: 17 307.3 cm^{-1}; 6: 16 995.2 cm^{-1} (compare Table 1).

Ab initio calculations on the optimized geometric structure using a Hartree–Fock (HF/6-31G(d)) and a density functional approach (B3LYP/6-31G(d)) (*21*) yielded values of 147 and 136 cm^{-1} for the lowest energy mode of PT respectively. In Ref. (*13*) a value of 132 cm^{-1} for ν_{18} was derived from scaled quantum-mechanical force field calculations. The calculated vibrational wavenumbers are somewhat smaller than our experimental value; a significantly better agreement, however, cannot be expected on the basis of ab initio calculations.

The Lowest Triplet State Mode $T_{1z,\nu_{18}}$ (b_1)

The weak band at 152.3 cm^{-1} forms the origin of a weak harmonic sequence and is the only possible mode in this spectral region which can be attributed to the lowest fundamental mode ν_{18} in the triplet state. It is not part of any strong progression in the spectrum. Its absorption was too weak to be observed in the supersonic jet measurements (compare Fig. 4). The spacing between the lines (orders) of most sequences, given in column 5 of Table 1, is expected to represent the energy difference of the mode $T_{1z,\nu_{18}}$ in the triplet and $S_{0,\nu_{18}}$ in the ground state. The sequence spacings found vary between −9 and −16.5 cm^{-1} with an average of −12.6 cm^{-1}. This value deviates by only 2.6 cm^{-1} from the value of −15.2 cm^{-1} found on the basis of our ν_{18} assignments: $\tilde{\nu}(T_{1z,\nu_{18}}) - \tilde{\nu}(S_{0,\nu_{18}}) = 152.3 - 167.5$ cm^{-1}. Moreover, if the assignments of $S_{0,\nu_{18}}$ and $T_{1z,\nu_{18}}$ are correct, then the sequences based on the vibronic origin at 16 678.9 cm^{-1} and the electronic origin at 16846.4 cm^{-1} (see Table 1) must involve the same states. Thus, the energy spacings of these two sequences should be very similar, which is indeed the case: spacings of −12.85 and −13.00 cm^{-1} were found for the two sequences, respectively (see Table 1). These arguments justify the assignment of $T_{1z,\nu_{18}} = 152.3$ cm^{-1}.

3.2. Comparison of Static PT Gas and Jet-Cooled PT

The low energy part of the cavity ring-down absorption spectrum of static PT gas is compared in Fig. 4 with the CRD absorption spectrum of jet-cooled PT and with the $T_1 \leftarrow S_0$ phosphorescence excitation spectrum of PT in a supersonic jet (cf. caption of Fig. 4). The relative absorbance scale of the static cell measurement (Fig. 4A) is greater than the scale of the

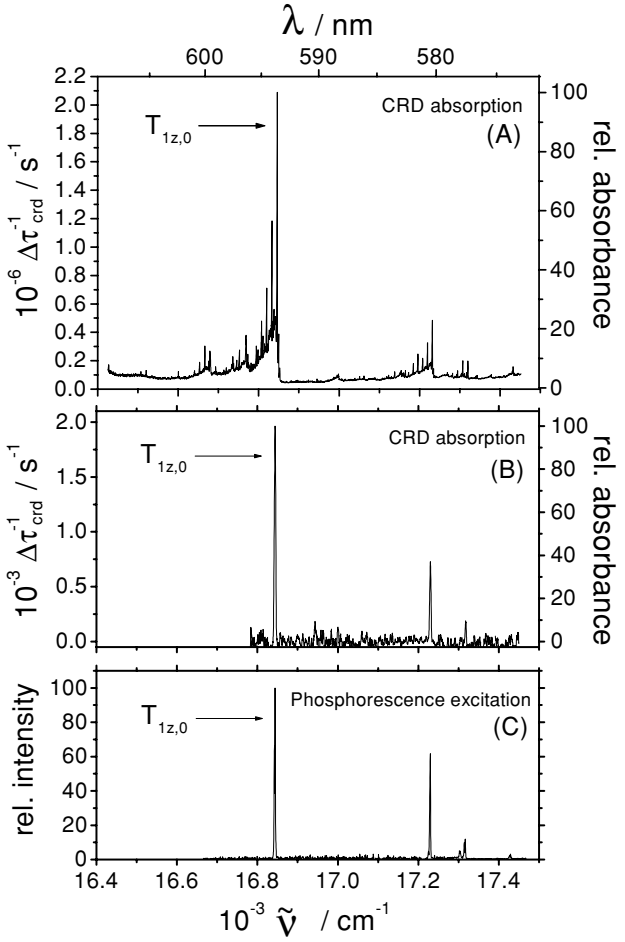

FIG. 4. Absorption region of the lowest vibronic transitions $T_{1z,\nu} \leftarrow S_0$ between 16 400 and 17 500 cm^{-1}. (A) Cavity ring-down absorption spectrum of PT in a static cell (T = 298 K). (B) Normalized cavity ring-down absorption spectrum of PT in a helium expansion (≈1000 mbar). This spectrum was slightly smoothed by averaging 3 adjacent points, which lowered the measured relative absorbances by ≲30%. (C) Normalized $T_1 \leftarrow S_0$ phosphorescence excitation (PE) spectrum of PT in a helium expansion (≈1000 mbar) from Ref. (*6*). All excitation wavenumbers are vacuum corrected.

jet-experiment (Fig. 4B) by a factor of ∼1000. This huge difference in the absorption signal is simply due to the vastly different number density in the two experiments. Even the weakest absorption features in the static cell spectrum are therefore real and reproducible. The CRD spectrum for jet-cooled PT,[3] however, shows a worse signal-to-noise ratio than the PE spectrum (Fig. 4C), due to the limitations of the mirror reflectivities and owing to the fact that the phosphorescence is detected against an effectively negligible background. Only the three strongest lines (0_0^0, ν_{27}, ν_{10}) could be observed in the CRD absorption spectrum of jet-cooled PT, whereas in the PE spectrum two additional (weak) lines were observable. The weakest line in Fig. 4C will be discussed in conjunction with the S_1 origin whose energy $S_{1,0}$ is not accurately known for *isolated* PT. The reason for the $S_{1,0}$ origin being difficult to observe is that PT does not show any prompt $S_1 \rightarrow S_0$ fluorescence (*1*). No emission is observed in jet-cooled PT after one-photon $S_1 \leftarrow S_0$ excitation, because the S_1 is effectively decoupled from T_1 (so-called small molecule limit). However, on the basis of the data presented and in comparison with measurements on BPT, we suggest the following tentative assignment of the absorption feature at ∼17433 cm^{-1} to be the $S_{1,0} \leftarrow S_{0,0}$ transition. Our assignment is based on the following arguments: (i) In BPT the energy gap $\Delta E(S_1, T_1)$ was found to be almost the same in the isolated molecule and in solution (*4*). In BPT the $S_{1,0}$ absorption was found to be 0.134 times as strong as the $T_{1z,0}$ absorption. Assuming a similar behavior in PT, the weak transition at 17 433 cm^{-1} in the CRD absorption spectrum (Fig. 4A) is only ≈14 cm^{-1} away from the energy gap $\Delta E(S_1, T_1) \approx 600$ cm^{-1} in solution. This weak line is 0.076 times as strong as the $T_{1z,0}$ absorption, which compares reasonably well with the finding for BPT. Owing to the higher symmetry a somewhat weaker $S_1 \leftarrow S_0$ transition can be expected for PT compared with BPT. (ii) In the phosphorescence excitation spectrum of jet-cooled PT the same weak feature was observed at an excess energy of 585 cm^{-1} above the T_{1z} origin. It is 0.032 times weaker than $T_{1z,0}$ (Fig. 4C). This feature was already tentatively attributed to the $S_{1,0} \leftarrow S_{0,0}$ transition in Ref. (*6*). The fact that it was observed at all in the phosphorescence excitation spectrum can be understood on the basis of a resonance-enhanced two-photon process as discussed in Ref. (*3*). After resonant two-photon absorption into the S_2 manifold subsequent ISC efficiently leads to the population of highly excited vibronic triplet states, from which a phosphorescence with an adequate quantum yield can be observed (*22*). (iii) In the FTIR spectrum of PT in the ground state (*13*) no normal vibration near 586 cm^{-1} was observed, which is also supported by ab initio (*21*) and SQM force field calculations (*13*). Furthermore, the line at ∼17433 cm^{-1} could not be assigned to any combination or sequence of the vibronic triplet states.

Additional assignments of vibronic states $S_{1,\nu}$ are virtually impossible because first, the static cell CRD spectrum of PT is too congested at higher excess energies and second, in the CRD jet experiment the signal-to-noise ratio was too small to allow the observation of the expectedly weak $S_{1,\nu} \leftarrow S_{0,0}$ absorption features.

3.3. The Rotational Envelope of the 0,0 Transition of PT

The large difference in the rotational temperature between the jet and the static cell measurement is demonstrated in Fig. 5, where the rotational envelope of the 0,0 transition in the jet is compared with that in static gaseous PT. The maximum in the static cell at 16846 cm^{-1} is shifted by ≈2 cm^{-1} with respect to the maximum wavenumber of the rotational envelope at 16844 cm^{-1} in a supersonic jet. The strongest central feature of $T_{1z,0}$ in the "warm" PT spectrum is narrower than the rotational

[3] The CRD spectrum of jet-cooled PT was slightly smoothed.

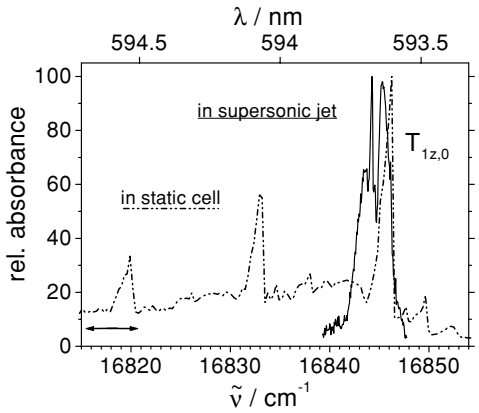

FIG. 5. (A) Comparison of the unresolved rotational structure in the region of the $T_{1z,0} \leftarrow S_{0,0}$ transition of jet-cooled PT ". . ." (A-type envelope) and of PT in a static cell "—," measured with the cavity ring-down method. The horizontal brace indicates the region where $T_{1(xy),0} \leftarrow S_{0,0}$ transitions would be expected.

envelope of PT in the cold jet. *In the static cell* (dashed line in Fig. 5) the shape of the observed structure is *determined by the density of states*, since at room temperature in thermal equilibrium the relevant rotational states in Fig. 5 are almost equally populated. The density of states increases dramatically near the rotational band edge leading to the observed shape. *In the molecular jet*, however (solid line in Fig. 5), the shape of the envelope is *determined by the population* of the rotational states according to the rotational temperature achieved in the molecular expansion. The shape is convoluted with the laser bandwidth of $\delta\tilde{\nu}_{\text{laser}} \lesssim 0.3$ cm, which is slightly larger than the Doppler broadening in the unskimmed jet (see Section 2) and thus represents the resolution limit of the measurement.

The results presented in this paper are a first step to study the outgasing of volatile materials with environmental relevance. Through the static cell experiment we have shown that the outgasing of materials can be monitored, even quantitatively. This will be particularly interesting for volatile solid materials of toxicological significance. Especially compounds with very low emission quantum yields but reasonably strong absorption transitions in the IR and near IR could be monitored successfully using the CRD technique. By going from lab to field conditions, the outgasing of relevant materials can be studied time- and temperature-dependent in analytical applications.

ACKNOWLEDGMENTS

We thank Dr. B. Nickel (to whom this publication is dedicated) and Dr. E. Tauer (MPI für Biophysikalische Chemie, Göttingen, Germany) for providing us with pure PT and supporting the measurements of the PT vapor pressure. This work was funded by the Irish organization for science and innovation FORBAIRT (Contract SC/97/755). A.A.R. gratefully acknowledges support by the German Research Council (DFG, Contract RU672/1-1/2/3) and by the Verband der Chemischen Industrie. Subsidies in support of T.F., granted by the European Leonardi Da Vinci program, are also gratefully acknowledged.

REFERENCES

1. A. Maciejewski and R. P. Steer, *Chem. Rev.* **93,** 67 (1993), and references therein.
2. A. A. Ruth, F. J. O'Keeffe, R. P. Brint, and M. W. D. Mansfield, *Chem. Phys.* **217,** 83 (1997).
3. A. A. Ruth, F. J. O'Keeffe, M. W. D. Mansfield, and R. P. Brint, *Chem. Phys. Lett.* **264,** 605 (1997).
4. A. A. Ruth, T. Fernholz, R. P. Brint, and M. W. D. Mansfield, *Chem. Phys. Lett.* **287,** 403 (1998).
5. A. O'Keefe and D. A. G. Deacon, *Rev. Sci. Instrum.* **59,** 2544 (1988).
6. A. A. Ruth, F. J. O'Keeffe, M. W. D. Mansfield, and R. P. Brint, *J. Phys. Chem. A* **101,** 7735 (1997).
7. M.-R. Taherian and A. H. Maki, *Chem. Phys. Lett.* **96,** 541 (1983).
8. A. Maciejewski, A. Safarzadeh-Amiri, R. E. Verrall, and R. P. Steer, *Chem. Phys.* **87,** 295 (1984).
9. A. Maciejewski, M. Szymański, and R. P. Steer, *J. Phys. Chem.* **90,** 6314 (1986).
10. M. J. Petrin, S. Ghosh, and A. H. Maki, *Chem. Phys.* **120,** 299 (1988).
11. M. Szymański, A. Maziejewski, and R. P. Steer, *Chem. Phys.* **124,** 143 (1988).
12. J. Tatchen, M. Waletzke, C. M. Marian, and S. Grimme, *Chem. Phys.* **264,** 245 (2001).
13. Á. Somogyi, G. Jalsovszky, C. Fülöp, J. Stark, and J. E. Boggs, *Spectrochim. Acta, Part A* **45,** 679 (1989).
14. G. Berden, R. Peeters, and G. Meijer, *Int. Rev. Phys. Chem.* **19,** 565 (2000).
15. K. W. Busch and M. A. Busch (Eds.), "Cavity-Ringdown Spectroscopy. An Ultra-Trace-Absorption Measurement Technique," Amer. Chem. Soc. Sympos. Ser., Vol. 720. Oxford Univ. Press, Oxford, 1999.
16. M. D. Wheeler, S. M. Newman, A. J. Orr-Ewing, and M. N. R. Ashfold, *J. Chem. Soc. Faraday Trans.* **94,** 337 (1998).
17. J. J. Scherer, J. B. Paul, A. O'Keefe, and R. J. Saykally, *Chem. Rev.* **97,** 25 (1997).
18. F. Arndt, E. Scholz, and P. Nachtwey, *Ber. Deutsch. Chem. Gesell.* **57,** 1903 (1924).
19. G. W. M. Thomson, *Chem. Rev.* **38,** 1 (1946).
20. G. Herzberg, "Molecular Spectra and Molecular Structure. III. Electronic Spectra and Electronic Structure of Polyatomic Molecules." Van Nostrand, Princeton, NJ, 1966.
21. M. J. Frisch, G. W. Trucks, H. B. Schlegel, G. E. Scuseria, M. A. Robb, J. R. Cheeseman, V. G. Zakrzewski, J. A. Montgomery, Jr., R. E. Stratmann, J. C. Burant, S. Dapprich, J. M. Millam, A. D. Daniels, K. N. Kudin, M. C. Strain, O. Farkas, J. Tomasi, V. Barone, M. Cossi, R. Cammi, B. Mennucci, C. Pomelli, C. Adamo, S. Clifford, J. Ochterski, G. A. Petersson, P. Y. Ayala, Q. Cui, K. Morokuma, D. K. Malick, A. D. Rabuck, K. Raghavachari, J. B. Foresman, J. Cioslowski, J. V. Ortiz, B. B. Stefanov, G. Liu, A. Liashenko, P. Piskorz, I. Komaromi, R. Gomperts, R. L. Martin, D. J. Fox, T. Keith, M. A. Al-Laham, C. Y. Peng, A. Nanayakkara, C. Gonzalez, M. Challacombe, P. M. W. Gill, B. Johnson, W. Chen, M. W. Wong, J. L. Andres, C. Gonzalez, M. Head-Gordon, E. S. Replogle, and J. A. Pople, "Gaussian 98, Revision A.3." Gaussian, Inc., Pittsburgh, 1998.
22. A. A. Ruth, W. G. Doherty, and R. P. Brint, *Chem. Phys. Lett.* **352,** 191 (2002).